Development of zero discharge net flow fluid dynamic gauging for studying biofilm and spore removal

Wang, S, Xu Zhou, K, Christie, G. and Wilson, D.I.

Department of Chemical Engineering and Biotechnology, Philippa Fawcett Drive, Cambridge, CB3 0AS, UK

Submitted to

Food & Bioproducts Processing

August 2018

Corresponding author

D. Ian Wilson

Department of Chemical Engineering and Biotechnology

Philippa Fawcett Drive

Cambridge

CB3 0AS

UK

Tel +44 1223 334 791

E-mail diw11@cam.ac.uk

Development of zero discharge net flow fluid dynamic gauging for studying biofilm and spore removal

Wang, S, Xu Zhou, K, Christie, G. and Wilson, D.I.

Department of Chemical Engineering and Biotechnology, Philippa Fawcett Drive, Cambridge, CB3 0AS, UK

Abstract

The fluid dynamic gauging (FDG) technique was originally developed to monitor the thickness of soft fouling layers immersed in liquid to provide quantitative information on fouling and cleaning processes. The latest version of the technique, scanning zero net flow FDG, allows measurements to be made aseptically at different locations on the same sample. Its potential for studying the removal of high-risk soils is demonstrated in (*i*) quantifying the shear stress required to remove bacterial spores from glass and stainless steel, and (*ii*) measuring the rate of erosion of *Rhodopseudomonas palustris* biofilms from standard and graphene-coated carbon paper. The adhesion of *Bacillus cereus* and *B. megaterium* spores was shown to differ significantly between spore type, spore cultivation conditions and substrate. The characteristic shear stresses required to remove 50% of the spore lawns were significantly greater than those imposed by standard industrial pipe flows. The *R. palustris* biofilms were uneven, with thicknesses ranging from 120±37 to 280±98 μm. The manner and rate of biofilm erosion was again strongly dependent on substrate. A new erosion modelling approach is presented which quantifies the differences in the biofilms in terms of erosion rate and strength. Biofilms grown on graphene were thinner, eroded more quickly and exhibited low adhesion strength.

Keywords Adhesion, biofilms, cleaning, removal, spores, substrate.

Introduction

Cleaning-in-place systems often employ solutions of cleaning agents, which convert the soil or deposit layer to a softer form, promoting erosion or the detachment of the layer from the underlying substrate by modification of the adhesive interactions between the soil and the substrate. Measuring the changes in soil dimensions (such as those promoted by swelling) and mechanical strength, in real time, while the soil is immersed in liquid is often challenging, and prompted the development of the fluid dynamic gauging technique (FDG, see Tuladhar *et al*., 2000). In FDG, the location of the soil-liquid interface is calculated from the pressure drop across a converging nozzle located in the liquid near the interface at a known flow rate. Figure

1(*a*) illustrates the FDG configuration: h is the nozzle – soil gap (or clearance) and d_t is the nozzle throat diameter. Measurements of the pressure drop and flow rate allow the nozzle discharge coefficient, C_d, to be calculated and this parameter is very sensitive to h/d_t when $h/d_t < 0.25$ (see Tuladhar *et al*., 2000). Knowledge of the location of the nozzle relative to the substrate allows the position of the interface to be calculated and thus any changes over time or resulting from fluid shear determined.

FDG can operate with the pressure drop set and flow rate measured (*e.g*. Tuladhar *et al*., 2000) or vice versa, with the pressure drop measured (e.g. Yang *et al*., 2014). The latter mode of operation results in FDG devices occupying a significantly smaller footprint than the original apparatuses, and allows the thickness and strength of the fouling layer to be determined at several locations when employed in a scanning mode. By using syringe pumps to introduce or withdraw fluid at a fixed or adjustable rate in an alternating sequence, the total volume of solution does not change, thereby achieving zero net flow (giving ZFDG, see Yang *et al*., 2014). This enables aseptic operation, as well as supporting testing with solutions of high value or significant safety risk (Wang *et al*., 2016). The photograph in Figure 1(b) shows the ZFDG unit used in the work on biofilms reported here. The footprint of the device is approximately 300×300 mm^2, with a similar area required for the syringe pump.

Gauging is performed with liquid flows in the creeping or inertial regimes, so the shear stress imposed on the substrate-liquid or layer-liquid interface can be calculated using computational fluid dynamics (CFD) simulations (see Yang *et al*., 2014; Wang *et al*., 2015) or estimated with reasonable confidence by treating the region under the nozzle rim as a viscous flow between parallel discs. The $C_d - h/d_t$ characteristics differ between suction and ejection modes, and CFD studies have quantified the influence of mode on the shear stress imposed on the soil-liquid interface (Wang *et al*., 2016). Figure 1(*c*) shows the good agreement which can be achieved between fluid flow simulations and experimental measurements.

The ZFDG concept has been developed as an open source technique and full details of the scanning ZFDG device are given in Wang *et al*. (2016). This paper reports novel applications of the ZFDG technique in studying the detachment of biofilms and spores. The applications are presented as individual case studies.

Adhesion of spores

The removal of bacterial spores from surfaces is a challenge in the food, medical and military sectors (Rönner and Husmark, 1992; Andersson *et al*., 1995) and CIP applications require knowledge of the force of adhesion between the spore and the substrate in the immersed state. Particle and spore adhesion measurements have been made with radial flow cells (*e.g*. Shah *et al*., 2007; Detry *et al*., 2009; Touré *et al*., 2014) and with atomic force microscopy (*e.g*. Bowen *et al*., 2002). One advantage of the ZFDG device is that in scanning mode measurements can be made at different locations on the same sample, providing consistency within data sets.

Method

Spore lawns were prepared on 50 mm diameter 316 stainless steel or microscopy-grade borosilicate glass discs using the technique reported by Xu Zhou *et al*. (2017a). Spores were applied as a slurry and left to rest for 5 to 10 minutes. The disc was then spun at 250 rpm, to remove excess water, and simultaneously dried with a hair drier. Once the central area of the coupon became visibly dry, the remaining liquid on the disc was spun off at high speed (>2000 rpm). Each sample was visually inspected to ensure coating smoothness and uniformity. Results are reported for two spore types, *B. cereus* 569 and *B. megaterium* QM B1551, cultured under neutral and alkali (pH 9) conditions since the effect of culture conditions is known to affect the properties of the spores (Xu Zhou *et al*., 2017b).

FDG testing was performed with deionised water at 20°C and pH 7. The nozzle was moved into position and deionised water at pH 7 and 20°C ejected at 0.8 mL s^{-1} for 2 minutes using a syringe pump, effectively emptying the barrel. A fraction of the spores detached on contact with water, when the contact line changed from substrate-spore-air to substrate-spore-water, and these are labelled ‘weakly adherent’. The nozzle was then moved away from the substrate, the barrel recharged and the substrate moved using a computerised *x-y* stage to the next location. Between 6 and 14 locations were tested on a disc, after which it was removed from the liquid and dried.

Figure 2 shows examples of plates before and after gauging at several locations. Optical microscopy was used to generate high magnification images (400×) of the gauged sites (the craters in Figure 2(b)). ImageJ (NIH, Bethesda, MD) was used to count the spores on the plate before immersion and in the annular region beneath the nozzle rim after gauging, labelled N_o

and N, respectively. The average shear stress imposed on the rim region, $\underline{\tau}_{wall}$, was calculated from

$$\underline{\tau}_{wall} = \mu \frac{3Q}{4\pi(h/2)^2} \frac{2}{(r_1 + r_2)} \quad [1]$$

where Q is the volumetric flow rate of liquid and μ is its viscosity; r_1 is the inner radius of the nozzle and r_2 the outer radius, with $r_1 = d_t/2$ and $r_2 = r_1 + w_r$. The gauging nozzle used in this work featured d_t = 1 mm and w_r = 0.5 mm.

Testing a number of locations with different shear stresses yields an adhesion profile relating the fraction of spores remaining on the surface, N/N_0, to $\underline{\tau}_{wall}$. The adhesive properties of the spore population were assumed to be normally distributed, so that the fraction of spores remaining on the surface could be fitted to

$$\frac{N}{N_0} = 1 - \sqrt{\frac{1}{2\pi\sigma^2}} \int_0^{\underline{\tau}_{wall}} exp\left(-\frac{(\tau - \tau_{50})^2}{2\sigma^2}\right) d\tau \quad [2]$$

Here τ is the wall shear stress in the region of interest and σ is the standard deviation from the mean value, τ_{50}, required to detach 50% of spores from the substrate. The τ_{50} and σ values were obtained by fitting the (N/N_0) vs. $\underline{\tau}_{wall}$ data to the above expression.

Results

Figure 3 shows that the data fitted the normal distribution model reasonably well. The parameters obtained are summarised in Table 1. There are evident differences in adhesion between spore species and substrate. *B megaterium* adhered to both surfaces, with low (≤ 14%) amounts being weakly adherent, and could be removed by fluid shear.

The τ_{50} values on stainless steel were 2× higher for both strains considered, indicating that more severe flow and chemistry conditions would be required for CIP on the steel. It should be noted that a τ_{50} value of 52 Pa would require a water flow velocity of approximately 4.5 m s^{-1} if the Fanning friction factor was 0.005. Kinetic testing, whereby the spores were subjected to the flow for different times, was not conducted here and represents a topic for future work.

Whereas both *B. megaterium* forms could be removed from glass and stainless steel, the FDG test was not able to remove the pH 7 variant of *B. cereus* from stainless steel and the pH 9

variant from the glass. For the pH 7 variant on glass and pH 9 variant on steel, the fractions of weakly adherent spores were significant (around 40%) but the magnitude of the τ_{50} values, at 160 Pa and 380 Pa respectively, lie beyond the range of normal CIP operating conditions, so that the majority of the spores would not be removed by hydraulic forces alone. These results demonstrate that spore adhesion characteristics vary widely between and within species as well as with the substrate, such that CIP programmes need to be tailored to the spore type(s) likely to be encountered.

Additionally, the impact of extended drying time on the adhesion strength of *B. megaterium* spores to glass is shown in Figure 4. The τ_{50} for spores dried in air for 24 hours more than doubled compared to when gauged immediately following sample preparation (114 vs 52 Pa). These results indicate that extended periods of drying make it significantly more challenging to remove bacterial spores, and therefore highlights the importance of minimising drying time prior to starting cleaning procedures.

Erosion of biofilms

Erosive removal

FDG has been used to measure the thickness of biofilms *in situ* (*e.g.* Salley *et al*., 2012; Lemos *et al*., 2016). The ZFDG can also be used to monitor the change in biofilm thickness, δ, in real time. The nozzle is held at a fixed position: as the biofilm is eroded the clearance, h, increases and the shear stress exerted on the layer decreases. Knowing how the wall shear stress depends on h for a set flow rate, the gauging data can be used to model the erosion of the layer being gauged.

A series of CFD simulations were used to determine how the peak wall shear stress τ_m varies with h over the range of values encountered in the experiments, and the data fitted to a relationship of the form (see Figure 5):

$$\tau_m = \frac{a}{h^b} \qquad [3]$$

The values of a and b obtained from this fitting are reported in Table 2. The layer thickness is assumed to decrease evenly and the rate of erosion is modelled as being first order in τ_m, with rate constant, k, viz.

$$\frac{d\delta}{dt} = -k\tau_m \qquad [4]$$

where t is time exposed to the eroding shear flow. The nozzle is fixed in position and the same gauging flow rate is used in the eroding stage, fixing a, b and h_o for that test. Since $\delta = h_o - h$, [4] becomes

$$\frac{dh}{dt} = \frac{ak}{h^b} \qquad [5]$$

with solution

$$h^{b+1} = (h_0 - \delta_0)^{b+1} - a(b+1)kt \qquad [6]$$

As the layer erodes, h increases and the rate of erosion decreases. Estimates of the erosion rate constant were obtained by fitting the experimental data to the above expression.

This is an approximate model as the shear stress imposed by the gauging flow is not uniform, and decreases with increasing r. The shape of the eroded region will therefore change with time and position. A more accurate physical model would require detailed simulations of the

coupled deformation problem capturing the evolution of the biofilm and its impact on the gauging flow hydrodynamics, supported by measurements of the biofilm morphology.

Biofilm formation and measurement

Rhodopseudomonas palustris biofilms were grown on two conducting substrates, namely carbon paper (CP) and graphene coated carbon paper (CPG). These biofilms were being considered as potential components of biophotovoltaic (BPV) systems (see McCormick *et al*., 2011), in which the cohesive strength of the biofilm and its adhesion to the substrate are important characteristics. Graphene consists of sp2 hybridised carbon in thin sheets which afford it superior strength, electrical and thermal conductivity properties (Sur, 2012). Graphene coating has been postulated to promote BPV activity via graphene's higher electrical conductivity. The adhesive force between the biofilm and the solid substrate, however, is also significant. The ZFDG system in Figure 1(*b*) was used to measure the thickness of biofilm at several points on each sample, the shear stress required to remove the biofilm, and the rate of biofilm erosion. The BPV activity on the two substrates is reported in a separate paper (Call *et al*., 2017).

Carbon paper (thickness 0.3–0.5 mm, roughness approximately 10 μm) was glued on 316 SS discs (diameter 50 mm, thickness 3 mm). The steel layer provided stiffness for support during transport. Graphene substrates were prepared by coating graphene film on top of a carbon paper substrate. This was performed by colleagues at the University of Cambridge Graphene Centre. All the surfaces had an approximate roughness of 10 μm. *Rhodopseudomonas palustris* biofilms were prepared on the carbon paper and graphene coated carbon paper substrates, immersed in extra growth media (minimal medium with 40 mM glycerol as carbon source and 5 mM urea as nitrogen source, Gosse *et al*, 2007) and shaken gently for 7 days at 50 rpm at 17°C and ambient light condition to promote biofilm formation.

The ZFDG system in Figure 1(*b*) was used for these tests. The cylindrical reservoir (height 150 mm, diameter 130 mm, operating volume in these tests = 2 L) was constructed from Perspex™ so that the layer could be monitored visually during testing. The nozzle and piping were 304 or 310 stainless steel. A detailed description of the device is given in Wang *et al*. (2016). The system could be isolated by means of a flexible polypropylene film which was secured to the

top edge of the reservoir and to a ring on the nozzle mounting. The nozzle passed through a septum on the latter ring, providing a gas-tight seal. The airspace within the tent could be isolated, exchanged or purged as necessary. The flexibility of the film allowed it to change shape as the liquid level changed when the gauging fluid was withdrawn or added to the reservoir via the nozzle, and adjusted with any transverse motion.

Liquid was fed by a computer controlled syringe pump (Hamilton® Glass, syringe i.d. =32.6 mm; Harvard Apparatus PHD UltraTM Series). The accuracy in the flow rate was measured as 1% of the set value. The nozzle vertical position was controlled by a stepper motor (Zaber Technologies, model T-LSR075B). Displacement in the horizontal plane was provided by a motorised *x*-*y* stage (travel 75 mm × 75 mm, resolution 2.5 μm; STANDA). The pressure drop across the nozzle was measured by a pressure transducer (SensorTechnics HMAP001BU7H5) with an operating limit of approximately 7 kPa. Examples of the $C_d - h/d_t$ characteristics, and associated CFD simulations, are shown in Figure 1(*c*). Details of the CFD calculations are given in Wang *et al*. (2016).

Testing was conducted at 16.5°C. The biofilms were transferred into buffer solution and buffer solution used as a gauging liquid. System control, data collection and processing were performed with a LabVIEW® (National Instruments^{TM}) application.

The initial thickness of the biofilm, δ_0, was determined by FDG measurement with a low liquid flow rate, of 5 mL/min. The nozzle was then moved to approximately 0.1 mm from the biofilm/liquid interface and liquid was ejected at a set flow rate for 4 s, followed by a 4 s period of no flow. This allowed the thickness to be measured, before testing again. The test was repeated at several other locations on each plate so that the influence of the variability of the biofilm could be assessed. The results in Table 3 shows that the biofilms grown on graphene were not as thick as those grown on carbon paper.

The plots of thickness against time subjected to the eroding flow in Figure 6 show a reduction in thickness over time for each biofilm which fitted Equation [6] well. Each thickness profile features a discontinuity, which corresponded to the formation of craters in the biofilm grown on carbon paper and complete removal (adhesive failure) on the graphene coated carbon paper. The associated shear stresses were labelled τ_C and τ_R, respectively. There was a noticeable effect of substrate on the shear stress causing deformation: on carbon paper, $\tau_C > 100$ Pa whilst on graphene τ_R was < 30 Pa. Figure 7 shows that τ_C increased almost linearly with initial biofilm thickness, which is consistent with this mode of deformation being related to the cohesive

strength (and thus amount) of the layer. There was no significant influence of δ_0 on τ_R, which is expected for adhesive failure between the substrate and a basal layer. Adhesive removal was not observed on the carbon paper substrates – these deformed by local cratering. These results indicate that the substrate affected the biofilm structure and interactions.

The parameters obtained from the tests are presented in Table 3. The erosion rate of the biofilms grown on the graphene coated surface was noticeably faster under similar shear stress conditions, yielding *k* values at least one order of magnitude larger than those obtained with the carbon paper. This indicates that the cohesive strength of the graphene biofilms was lower, reflecting the difference in adhesion strengths.

Figure 8 summarises these trends in plotting the erosion rate constant against the shear stress responsible for catering or peeling (adhesive failure). The two parameters cluster in different regions of the plot and confirm the difference in mechanical characteristics of the biofilms: those grown on carbon paper exhibited greater cohesive strength and erode more slowly.

Conclusions

The potential for the scanning ZFDG technique to be used to obtain previously difficult or inaccessible measurements has been demonstrated with two biological systems of interest to those working on cleaning and decontamination in several sectors.

The shear stress required to remove bacterial spores was estimated by making multiple measurements on a single substrate, spanning the range of shear stresses which can be reached in standard CIP processes. The results confirmed that spore adhesion is strongly affected by the species, substrate and sporulation conditions.

A new method for studying biofilm erosion is presented. The rate at which biofilms are eroded and the transition to bulk cohesive or adhesive failure was measured directly and the influence of the substrate on the biofilm structure and strength was confirmed.

Acknowledgements

KXZ was supported on an EPSRC Doctoral Training Grant and SW received a scholarship from Fitzwilliam College, Cambridge. Development of the FDG concept was supported by the

Royal Society's Paul Instrument Fund. The apparatus was constructed by the technical team at the Institute for Chemical and Thermal Process Engineering, TU Braunschweig, notably Karl Karrenführer, Jörg Leppelt and Sven Lorenzen. Biofilms were provided by Toby Call, Dr Paolo Bombelli and Prof. Chris Howe from the Algal Biotechnology Consortium at Cambridge. Funding for DIW to attend the FCFP2018 conference in Lund from Jesus College, Cambridge, is also gratefully acknowledged

OpenData Statement

The data presented in this paper will be available on the University of Cambridge Apollo data repository if the paper is accepted for publication. A link to the repository will be provided here.

References

Ali, A, Alam, Z, Ward, G. and Wilson, D.I. (2015) Using the scanning fluid dynamic gauging device to understand the cleaning of baked lard soiling layers, *J. Surf. Detergents*, **18**(6), 933-947.

Andersson, A., Rönner, U. and Granum, P. E. (1995) What problems does the food industry have with the spore-forming pathogens *Bacillus cereus* and *Clostridium perfringens*?, *Intl J. Food Microbiology*, **28**, 145-155.

Bowen, W. R, Fenton, A. S, Lovitt, R. W. and Wright, C. J. (2002) The measurement of Bacillus mycoides spore adhesion using atomic force microscopy, simple counting methods, and a spinning disk technique. *Biotech. Bioeng*, **79**, 170-179.

Call, T.P., Carey, T., Bombelli, P., Lea-Smith, D.J, Hooper, P, Howe, C.J. and Torrisi, F. (2017) Platinum-free, graphene based anodes and air cathodes for single chamber microbial fuel cells, *J. Matl. Chemistry A*, **5**, 23872-23886.

Detry, J.G, Jensen, B.B.B, Sindic, M. and Deroanne, C. (2009) Flow rate dependency of critical shear stress in a radial flow cell, *J. Food Eng*, 92, 86-99.

Gosse, J.L., Engel, B.J., Rey, F.E., Harwood, C.S., Scriven, E. and Flickinger, M.C. (2007) Hydrogen production by photoreactive nanoporous latex coatings of nongrowing *Rhodopseudomonas palustris* CGA009, *Biotechnol. Prog.*, **23**, 124–130.

Lemos, M, Wang, S, Ali, A, Simões, M.V. and Wilson, D.I. (2016) A fluid dynamic gauging device for measuring biofilm thickness on cylindrical surfaces, *Biochem. Eng*, **106**, 48-60.

McCormick, A.J., Bombelli, P., Scott, A.M., Philips, A.J., Smith, A.G., Fisher, A.C., and Howe, C.J., 2011. Photosynthetic biofilms in pure culture harness solar energy in a mediatorless bio-photovoltaic cell (BPV) system. *Energy & Environmental Sci.*, **4**(11), 4699.

Rönner, U. and Husmark, U. (1992) Adhesion of *Bacillus cereus* spores — a hazard to the dairy industry. In: Melo, L. F., Bott, T. R., Fletcher, M. & Capdeville, B. (eds.) *Biofilms — Science and Technology*. Springer, Netherlands.

Salley, B, Gordon, P. W, Mccormick, A. J, Fisher, A. C. and Wilson, D. I. (2012) Characterising the structure of photosynthetic biofilms using fluid dynamic gauging. *Biofouling*, **28**, 159-73.

Shah, F.A, Allen N, Wright, C.J. and Butt, T.M. (2007) Repeated *in vitro* subculturing alters spore surface properties and virulence of *Metarhizium* anisopliae, *FEMS Microbiol Lett*. **276**, 60-66.

Sur, U. K., 2012. Graphene: a rising star on the horizon of materials science. *Intl. J. Electrochemistry*, 12

Touré, Y, Genet, M.Y, Dupont-Gillain, C-C,Sindic, M. and Rouxhet, P.G. (2014) Conditioning materials with biomacromolecules: Composition of the adlayer and influence on cleanability *J. Colloid Interf. Sci*, **432**, 158-169.

Tuladhar, T.R, Paterson, W.R, Macleod, N. and Wilson, D.I. (2000) Development of a novel non-contact proximity gauge for thickness measurement of soft deposits and its application in fouling studies, *Can. J. Chem. Eng*, **78**, 935-947.

Wang, S, Schlüter, F, Gottschalk, N, Scholl, S, Wilson, D.I. and Augustin, W. (2016) Aseptic zero discharge fluid dynamic gauging for measuring the thickness of layers of soft solids on surfaces, *Chem. Ing. Tech*, **88**(10), 1530-1538.

Wang, S. and Wilson, D.I. (2015) Zero discharge fluid dynamic gauging for studying the swelling of soft solid layers, *Ind. Eng. Chem. Res*, **54** (32), 7859–7870.

Xu Zhou, K, Li, N, Christie, G.M. and Wilson, D.I. (2017a) Assessing the impact of germination and sporulation conditions on the adhesion of *Bacillus* spores to glass and stainless steel by fluid dynamic gauging, *J. Food Sci*, **82**(11), 2614-2625.

Xu Zhou, K, Wisnivesky, F, Christie, G.M. and Wilson, D.I. (2017b) Effects of culture conditions on the size, morphology and wet density of spores of *Bacillus cereus* 569 and *Bacillus* megaterium QM B1551, *Lett. Appl. Microbiology*, **65**, 50-56.

Yang, Q., Ali, A, Shi, L. and Wilson, D.I. (2014) Zero discharge flow fluid dynamic gauging for studying the thickness and removal of soft solid layers, *J. Food Eng*, **127**, 24–33.

Nomenclature

Roman

a	constant in Equation [3], Pa m^b
b	power law index in Equation [3], -
C_d	discharge coefficient, -
d_i	gauging tube internal diameter, m
d_t	nozzle throat diameter, m
h	clearance, m
h_o	distance from nozzle to substrate (clearance when clean), m
k	erosion rate constant, m $Pa^{-1}s^{-1}$
N, N_o	number of spores, intial number, -
P, P_0	pressure inside and outside gauging tube, Pa
Q	volumetric flow rate, m^3s^{-1}
Re_t	Reynolds number at throat, -
r_1	radial location of inner edge of nozzle rim, m
r_2	radial location of outer edge of nozzle rim, m
t	time, s
w_e	nozzle throat rim dimension (Figure 1(*a*)), m
w_r	nozzle throat rim width (Figure 1(*a*)), m
z	vertical co-ordinate direction

Greek

δ	biofilm or layer thickness, m
θ	internal angle, gauging nozzle, rad
μ	liquid viscosity, Pa s
ρ	liquid density, kg m^{-3}
σ	standard deviation, Pa
τ_C	shear stress associated with crater formation, Pa
τ_m	peak wall shear stress, Pa
τ_R	shear stress (adhesive failure), Pa
$\underline{\tau}_{wall}$	average shear stress imposed on rim region, Pa
τ_{50}	shear stress required to detach 50% of spores from substrate, Pa

Acronymns

BPV	biophotovoltaic
CFD	computational fluid dynamics
FDG	fluid dynamic gauging
ZFDG	zero net flow fluid dynamic gauging

Tables

Table 1 Summary of spore adhesion characteristics. Contact angle measured by sessile drop methods using on a spore lawn. τ_{50} values are reported as mean (standard deviation).

Spore type	contact angle	glass		316 stainless steel	
		weakly adherent	τ_{50} / Pa	weakly adherent	τ_{50} / Pa
B. megaterium, pH 7	101° ± 2	5%	52 (37)	1%	232 (228)
B. megaterium, pH 9	117° ± 3	4%	116 (49)	14%	226 (105)
B. cereus, pH 7	48° ± 2	38%	161 (234)	0%	> 1500
B. cereus, pH 9	114° ± 2	5%	> 1500	44%	383 (356)

Table 2. Power law parameters for dependency of maximum shear stress on clearance (Equation [3]) for water at 16.5°C by ejection. R^2 is the coefficient of determination.

Flowrate	Re_t	*a*	*b*	R^2
ml/min	-	$Pa.m^b$	-	-
5	94	0.20	1.72	0.996
6	113	0.26	1.70	0.996
7	132	0.33	1.68	0.996
8	151	0.40	1.66	0.995
9	170	0.48	1.65	0.995
10	189	0.57	1.63	0.994
20	377	1.65	1.53	0.988
30	566	3.12	1.47	0.984
40	754	4.88	1.43	0.981
50	943	6.92	1.41	0.979

Table 3. Summary of biofilm thickness measurements on carbon paper (CP) and graphene-coated carbon paper (CPG) substrates. Coverage is the area of the biofilm. *n* is the number of locations subjected to erosion testing. δ_{paper} is the total thickness of CP/CPG and biofilm, $\bar{\delta}$ the initial measured thickness of biofilm

Sample	Substrate Dimensions / mm	Coverage / mm^2	δ_{paper} / μm	Locations / -	$\bar{\delta}$ / μm	S.D. / μm
CP1	24.5 × 28.6	700	315	25	280	98
CP2	38.3 × 17.5	670	243	10	242	41
CPG1	11.2 × 11.3	127	338	6	121	37
CPG2	38.3 × 17.5	671	473	3	171	108

Figures

List of Figure captions

Figure 1 (*a*) Schematic of FDG nozzle operating with liquid ejection. P-P_0 is the pressure drop measurement. Geometrical features are labelled; distance h_0 is the nozzle-substrate separation. (*b*) Photograph of scanning ZFDPG device used in the biofilm studies reported here: (*i*) apparatus, and (*ii*) detailed view of 1 mm i.d. nozzle and substrate. Labels: M - motorised x-y stage, N - gauging nozzle, S - linear slide, T - gauging tank. (*c*) Examples of C_d- h/d_t relationships for ejection (E, open points, dashed line) and suction (S, solid points, line): calculated for the device in (*b*): points – experimental data, loci – CFD simulations [Source: Wang *et al*, 2016].

Figure 2 – Photographs of 50 mm diameter discs coated with *B. megaterium* spores. (*a*) stainless steel disc after drying and (*b*) glass disc after gauging in ejection mode at several locations using different clearance settings.

Figure 3 – Effect of average shear stress on the adhesion of spores of (*a*) *B. megaterium* and (*b*) *B. cereus* on (I) glass and (II) stainless steel. Symbols: △, *B. megaterium*; ◇, *B. megaterium*, cultured at pH 9; □, *B. cereus*; ○, *B. cereus* cultured at pH 9. Loci show the fit to Equation [2]. Reproduced from Xu Zhou *et al*. (2017a).

Figure 4 – Effect of drying time on the adhesion strength of *B. megaterium* spores to glass. Symbols: △, gauging immediately following disc sample preparation; ○, gauging 24 hours following disc sample preparation. Loci show the fit to Equation [2]

Figure 5 Effect of clearance on peak wall shear stress. Note logarithmic scale for τ_m. Liquid flow rate = 5 mL min^{-1} (circles, throat Reynolds number ($\equiv 4Q/\pi\mu d_t$) = 94), 20 mL min^{-1} (triangles, Reynolds number 380) or 50 mL min^{-1} (squares, Reynolds number 940).

Figure 6 Evolution of thickness of *Rhodopseudomonas palustris* biofilms on carbon paper (circles) and graphene coated carbon paper (triangles). Inset photographs show the samples after gauging. Scale bars indicate 10 mm length. Second y-axis shows data replotted in the form of equation [6]. Letter C indicates where the crater formation was first observed in the carbon paper sample, and R indicates where all the biofilm was removed from the nozzle footprint.

Figure 7. Effect of initial biofilm thickness, δ_0, on shear stress causing deformation for CP (hollow, τ_R) and CPG (solid, cratering, τ_C) substrates.

Figure 8 Log-linear plots of erosion rate constant, k, against onset of crater formation, τ_C, and adhesive removal, τ_R for carbon paper (hollow symbols) and graphene coated carbon paper (solid circles). Each datum indicates a local measurement. Marked regions indicate final different removal modes.

(*a*)

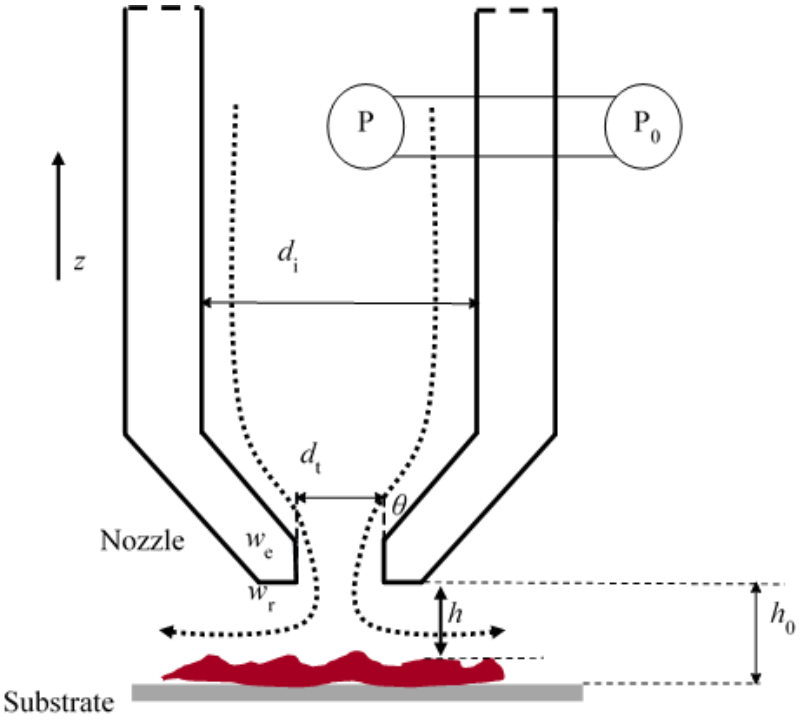

(*b*)

(*i*)

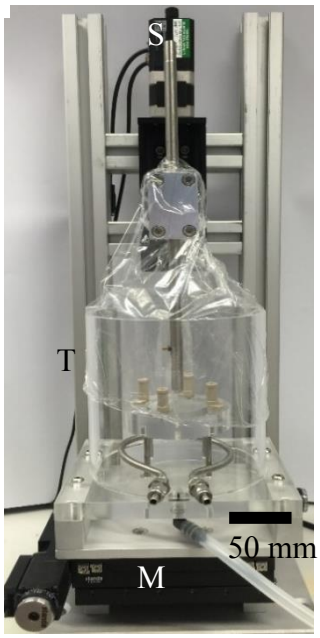

(*ii*)

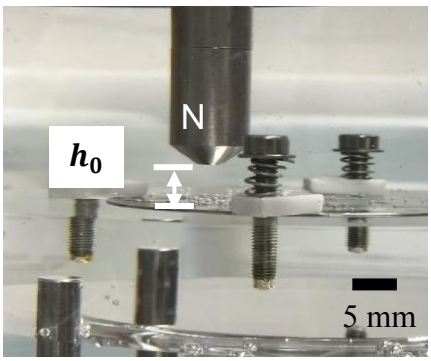

(*c*)

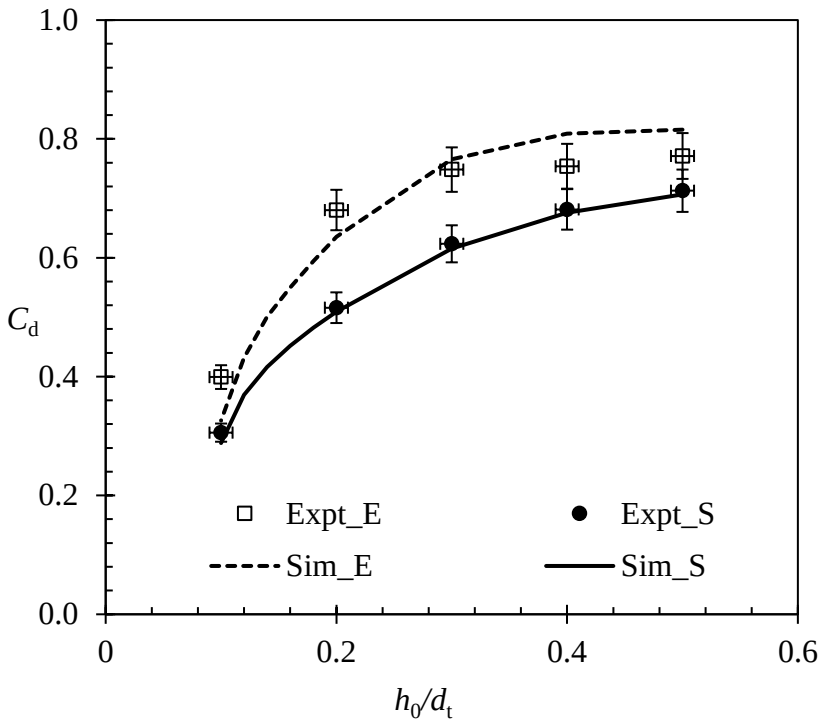

Figure 1 (*a*) Schematic of FDG nozzle operating with liquid ejection. P-P_0 is the pressure drop measurement. Geometrical features are labelled; distance h_0 is the nozzle-substrate separation. (*b*) Photograph of scanning ZFDPG device used in the biofilm studies reported here: (*i*) apparatus, and (*ii*) detailed view of 1 mm i.d. nozzle and substrate. Labels: M - motorised x-y stage, N - gauging nozzle, S - linear slide, T - gauging tank. (*c*) Examples of C_d- h/d_t relationships for ejection (E, open points, dashed line) and suction (S, solid points, line): calculated for the device in (*b*): points – experimental data, loci – CFD simulations [Source: Wang *et al*, 2016].

(*a*)

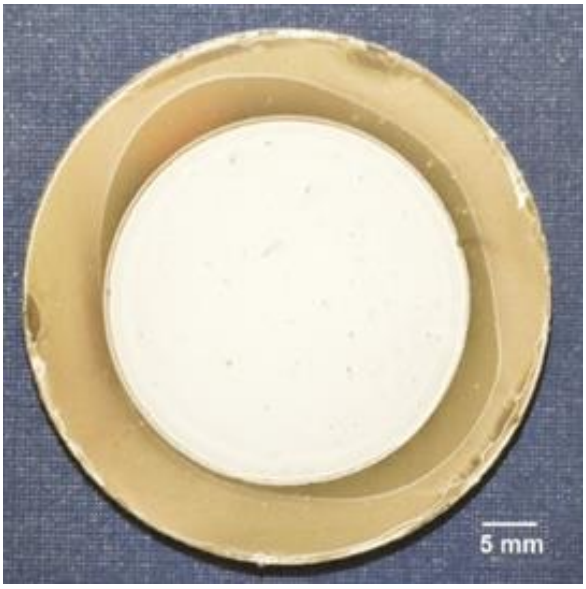

(*b*)

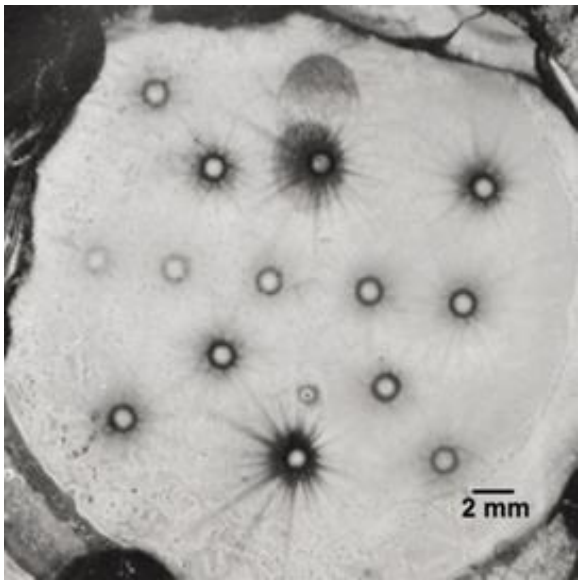

Figure 2 – Photographs of 50 mm diameter discs coated with *B. megaterium* spores. (*a*) stainless steel disc after drying and (*b*) glass disc after gauging in ejection mode at several locations using different clearance settings.

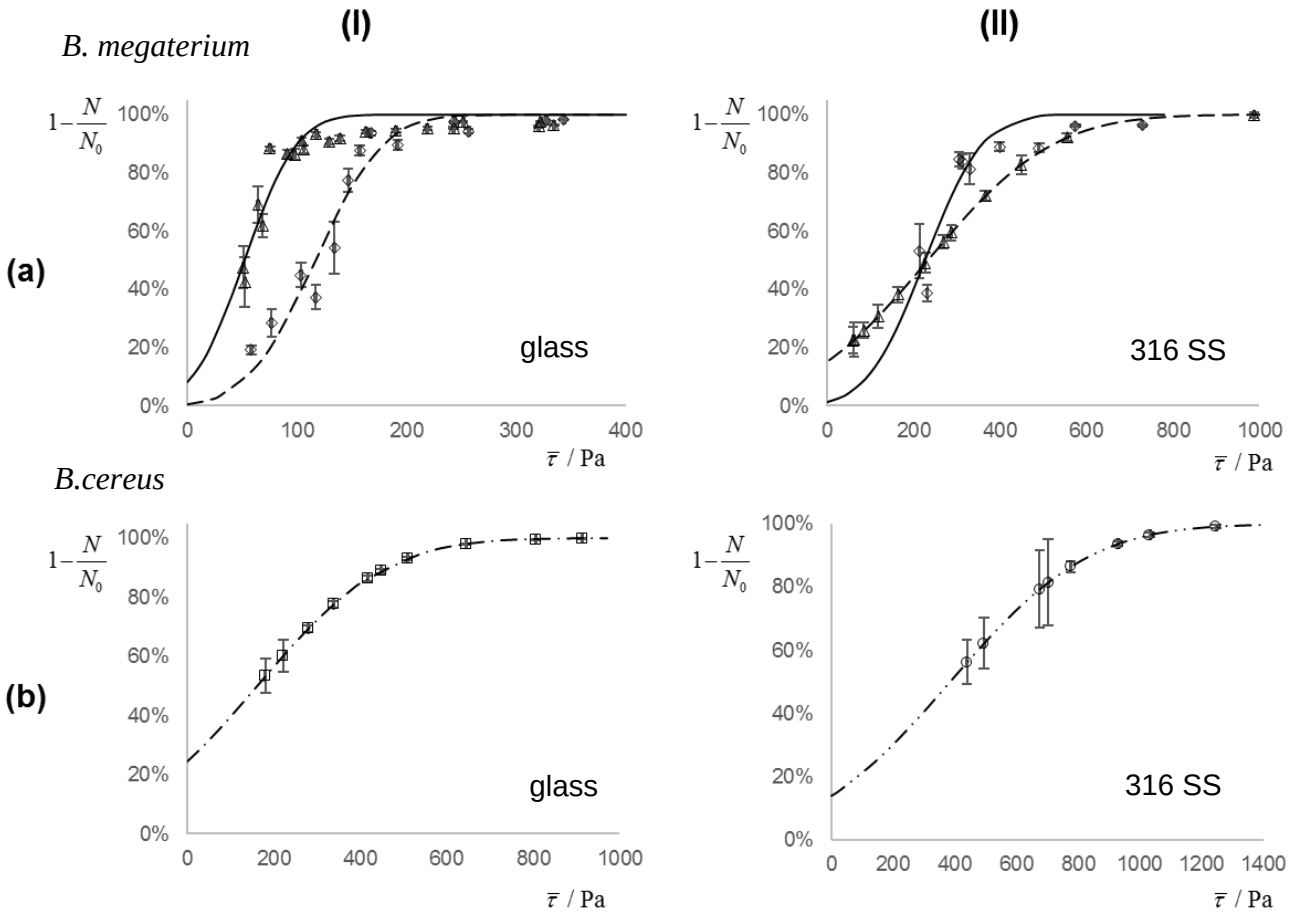

Figure 3 – Effect of average shear stress on the adhesion of spores of (*a*) *B. megaterium* and (*b*) *B. cereus* on (I) glass and (II) stainless steel. Symbols: △, *B. megaterium*; ◇, *B. megaterium*, cultured at pH 9; □, *B. cereus*; ○, *B. cereus* cultured at pH 9. Loci show the fit to Equation [2]. Reproduced from Xu Zhou *et al*. (2017a).

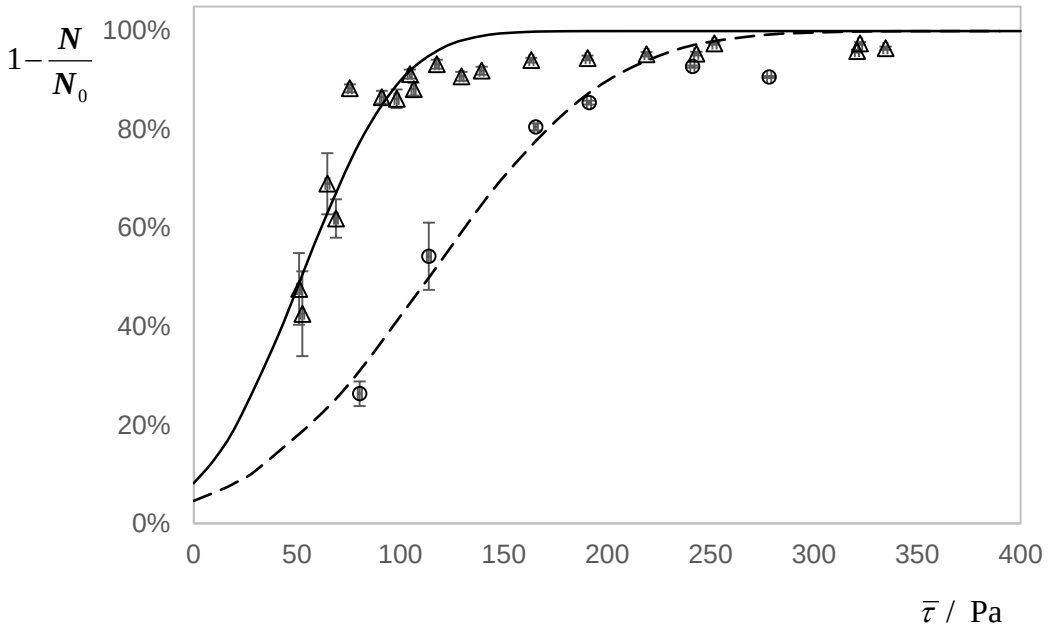

Figure 4 – Effect of drying time on the adhesion strength of *B. megaterium* spores to glass. Symbols: △, sample gauged immediately following disc sample preparation; ○, sample gauged after 24 hours of air drying following sample preparation. Loci show the fit to Equation [2]

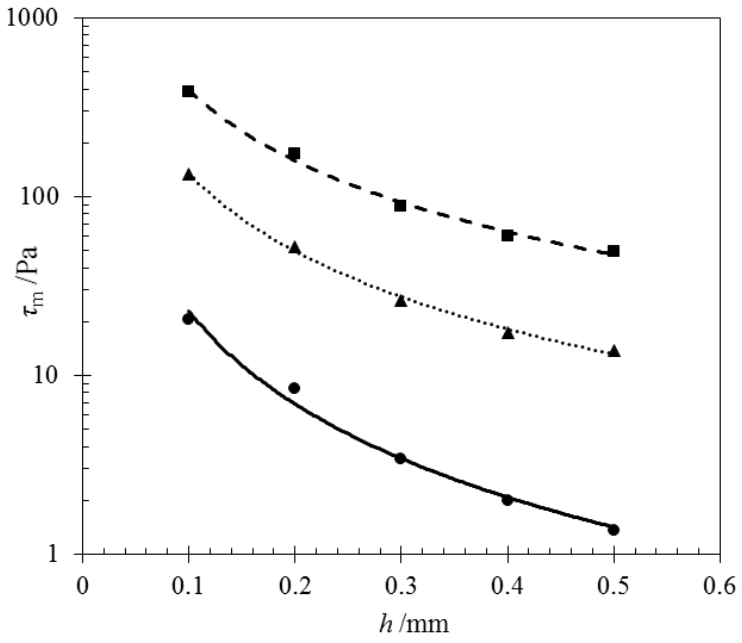

Figure 5 Effect of clearance on peak wall shear stress. Note logarithmic scale for τ_m. Liquid flow rate = 5 mL min^{-1} (circles, throat Reynolds number, $Re_t \equiv 4\rho Q/\pi\mu d_t = 94$), 20 mL min^{-1} (triangles, $Re_t = 380$) or 50 mL min^{-1} (squares, $Re_t = 940$) in ejection.

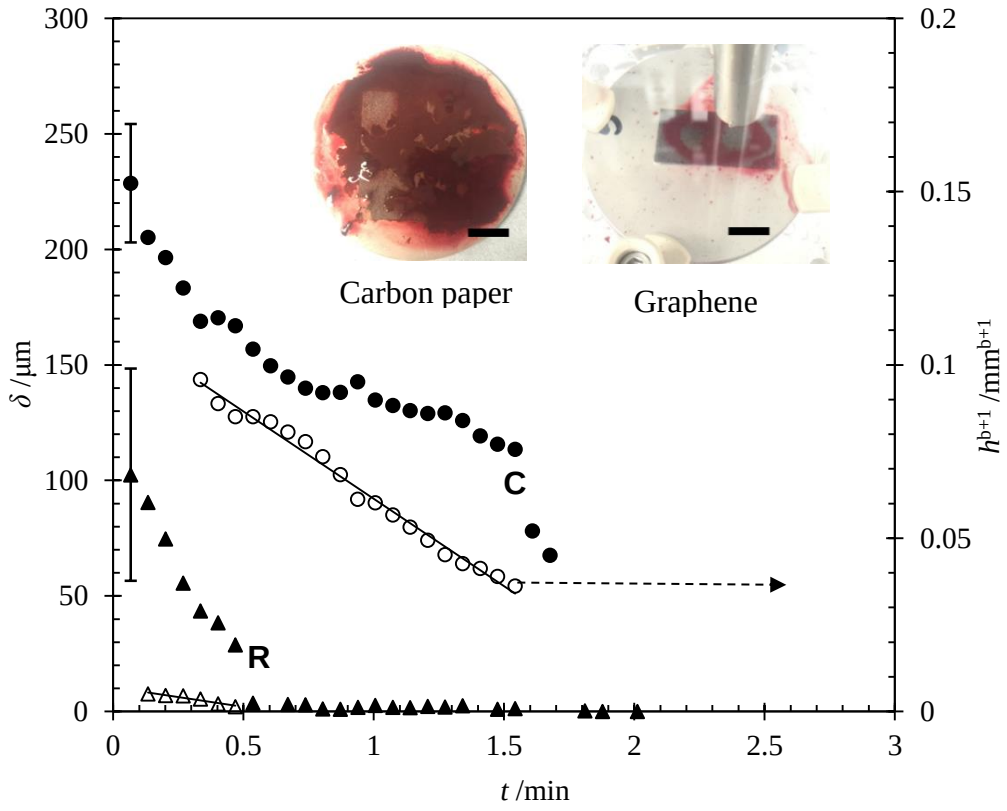

Figure 6. Evolution of thickness of *Rhodopseudomonas palustris* biofilms on carbon paper (circles) and graphene coated carbon paper (triangles). Inset photographs show the samples after gauging. Scale bars indicate 10 mm length. Second *y*-axis shows data replotted in the form of equation [6]. Letter C indicates where the crater formation was first observed in the carbon paper sample, and R indicates where all the biofilm was removed from the nozzle footprint.

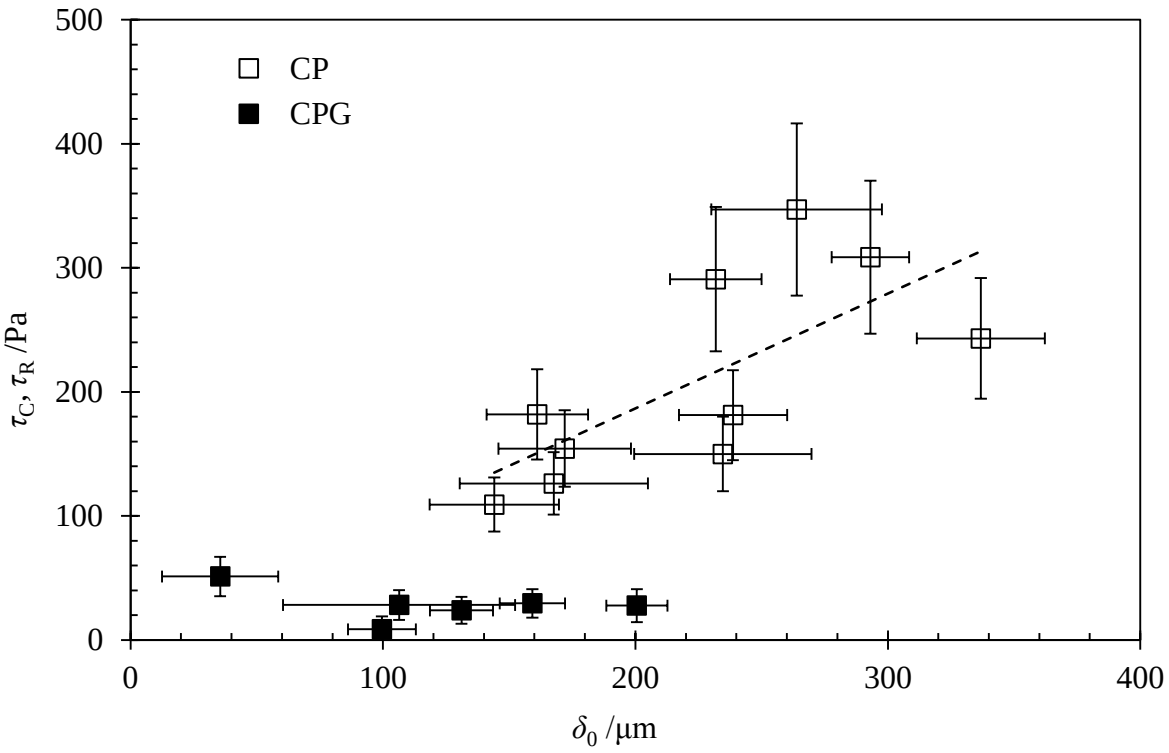

Figure 7. Effect of initial biofilm thickness, δ_0, on shear stress causing deformation for CP (hollow, τ_R) and CPG (solid, cratering, τ_C) substrates.

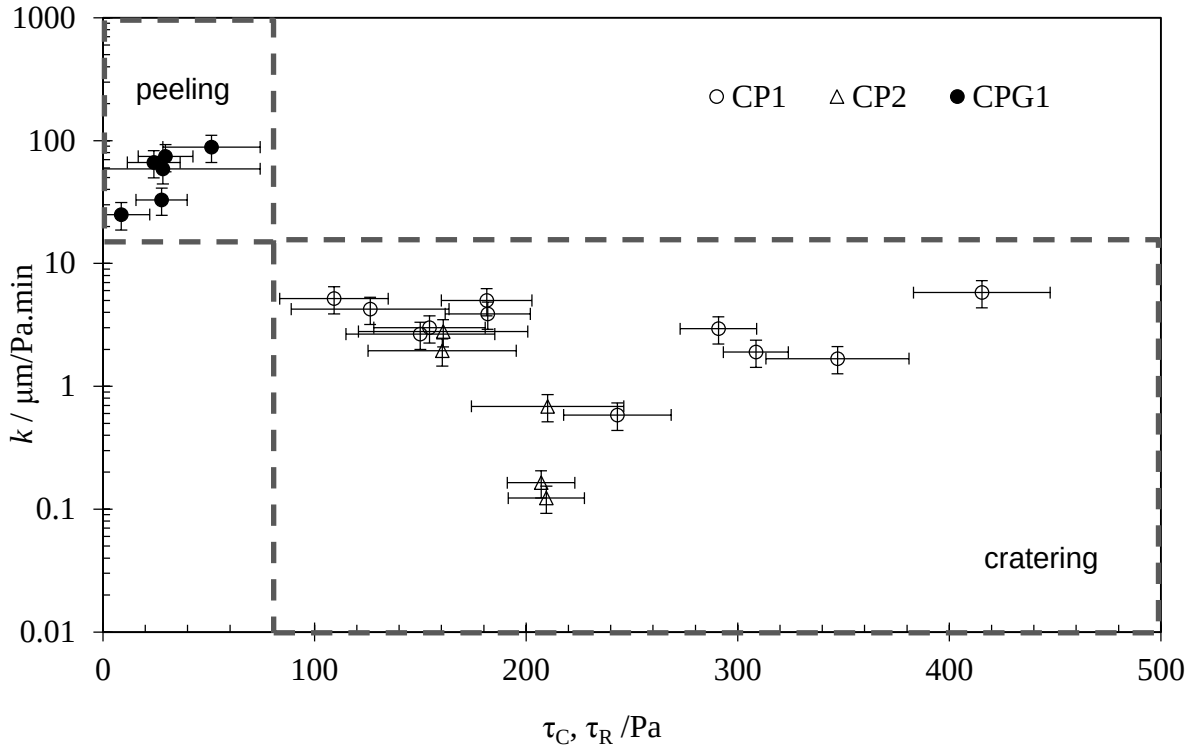

Figure 8 Log-linear plots of erosion rate constant, k, against onset of crater formation, τ_C, and adhesive removal, τ_R for carbon paper (hollow symbols) and graphene coated carbon paper (solid circles). Each datum indicates a local measurement. Marked regions indicate final different removal modes.